VIP Intermolecular Forces Very Important Paper

How to cite: *Angew. Chem. Int. Ed.* **2021**, *60*, 11305–11309
International Edition: doi.org/10.1002/anie.202016020
German Edition: doi.org/10.1002/ange.202016020

Dispersion-Bound Isolated Dimers in the Gas Phase: Observation of the Shortest Intermolecular CH···H–C Distance via Stimulated Raman Spectroscopy

Dominique Maué, Patrick H. Strebert, Dominic Bernhard, Sören Rösel, Peter R. Schreiner,* and Markus Gerhards†*

Abstract: *The triphenylmethane and all-meta tert-butyl triphenylmethane dimers, $(TPM)_2$ and $(T^tBuPM)_2$, respectively, were studied with ionization loss stimulated Raman spectroscopy in molecular beam experiments to resolve structure sensitive vibrations. This answers the question whether the recently reported linear head-to-head arrangement in $(T^tBuPM)_2$ results from crystal packing or prevails also in the gas phase, and therefore must result from extraordinarily strong London dispersion (LD) interactions. Our study clearly demonstrates that the head-to-head arrangement is maintained even under isolated molecular beam conditions in the absence of crystal packing effects. The central Raman-active aliphatic C–D vibration of appropriately deuterated $(T^tBuPM)_2$ associated with an unusually short C–D···D–C distance exhibits a strong blue-shift compared to the undisturbed case. As the LD stabilizing tert-butyl groups are absent in $(TPM)_2$, it displays an approximately S_6-symmetric tail-to-tail arrangement.*

London dispersion (LD) interactions[1] are of fundamental importance for many facets of chemistry and biology, yet they have been neglected for a long time[2] due to their supposedly "weak" nature. However, the latter is only true regarding individual interactions between two atoms, whereas the interaction strength grows rapidly with increasing size of the interacting molecules or moieties due to the (nearly) pairwise additivity.[3] This leads to significant steric attraction already for medium-sized molecules, becoming even the dominant factor determining the shape of supramolecular structures such as DNA[4] or proteins.[5] LD interactions furthermore explain macroscopic phenomena such as the existence of condensed matter and the remarkable adhesion effect of gecko setae,[6] utilized in glue research.

Another important and frequently disregarded aspect is the balance between Pauli repulsion and noncovalent attraction, which has recently been shown to be pushed towards the attractive side by utilizing "dispersion energy donors"[2,7] (DEDs), stabilizing unusual intra- or intermolecular bonding arrangements. Remarkable examples include, e.g., diamondoids connected via very long C–C bonds[8] as well as alkyl-substituted triphenylmethyl (TPM) derivatives[9] and all-*meta* *tert*-butyl hexaphenylethane.[10–12] The latter one is an extraordinary example of a sterically crowded system that nevertheless forms a stable molecule at room temperature exhibiting a melting point of 210 °C and of which even an X-ray structure could be obtained.[11] Conversely, unsubstituted hexaphenylethane is not stable despite the early assumption of its existence by Gomberg.[13] It rather equilibrates between the triphenylmethyl radical dimer, and a quinoid structure.[14] An explanation for the unexpected stability of $(T^tBuPM)_2$ originates from the enormous magnitude of LD interactions that outbalance Pauli repulsion.[10]

In order to gain insights into the intrinsic properties of these LD-bound systems (Figure 1), investigations at the molecular level are required without environmental effects. This can be achieved with molecular beam experiments, generating isolated molecules or defined molecular aggregates at low temperatures. Combining these experiments with, for instance, vibrational or rotational spectroscopy yields valuable structural information, as the spectra represent a fingerprint of the three-dimensional molecular structure, which can be compared to quantum chemical computations. Due to the low sample concentration in the molecular beam the measurement of direct light absorption is not

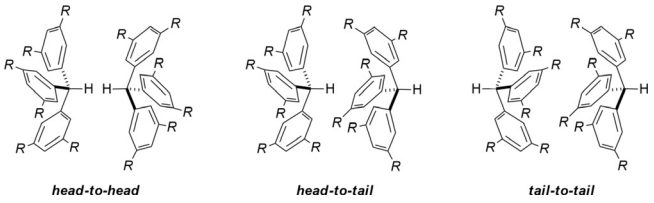

Figure 1. Different dimer motifs of triphenylmethane derivatives (R = H, ^{t}Bu).

[*] Dr. D. Maué, P. H. Strebert, Dr. D. Bernhard, Prof. Dr. M. Gerhards
Fachbereich Chemie and Research Center Optimas, TU Kaiserslautern
Erwin-Schrödinger-Str. 52, 67663 Kaiserslautern (Germany)
E-mail: ak_gerhards@chemie.uni-kl.de
Dr. S. Rösel, Prof. Dr. P. R. Schreiner
Institute of Organic Chemistry, Justus-Liebig University
Heinrich-Buff-Ring 17, 35392 Giessen (Germany)
E-mail: prs@uni-giessen.de
[†] Deceased 28.12.2020
Supporting information and the ORCID identification number(s) for the author(s) of this article can be found under: https://doi.org/10.1002/anie.202016020.

possible. Thus, action spectroscopic methods are performed, recording the effect of light (e.g., ionization with subsequent mass detection) on the molecule. An established powerful IR spectroscopic method is combined IR/UV spectroscopy[15] in combination with time-of-flight mass spectrometry. In the mass- and isomer-selective IR/R2PI method a vibrational excitation (via IR) is recorded as a depletion of an ion signal generated by resonant UV excitation followed by ionization via a second UV photon (R2PI = resonant two-photon ionization process, for details see SI).

Notwithstanding these technical advances, the structural analysis of symmetric molecules or aggregates is often hard or even impossible for infrared and/or rotational spectroscopy due to vanishing transition dipole moments or the lack of a permanent dipole moment. In such cases, Raman spectroscopy is an ideal method since such systems commonly exhibit highly Raman-active vibrational transitions. Spontaneous Raman scattering itself is an inefficient process in molecular beam experiments due to low sample concentrations in the gas phase. Stimulated Raman scattering[16] uses a pump/dump process, which increases the sensitivity by orders of magnitude. In analogy to the IR/R2PI method, stimulated Raman scattering can be combined with R2PI, a method labeled ionization loss stimulated Raman spectroscopy (ILSRS).[17] ILSRS allows a combination of vibrational spectroscopy and mass selectivity via time-of-flight mass spectrometry. In case of ILSR (see inset in Figure 2) the UV laser is set on an electronic transition within the corresponding R2PI spectrum, thereby generating a constant ion signal. A frequency-fixed pump photon ν_p depopulates the ground state (S_0) and the vibrational spectrum is obtained by monitoring the stimulated Raman-induced depletion of the ion signal as a function of ($\nu_p - \nu_s$) with ν_s being the wavenumber of the tunable Stokes photon. In addition to the ILSRS, ionization gain stimulated Raman spectroscopy (IGSRS)[18] is almost background-free since the ionization starts only from the vibrational states populated by the stimulated Raman process (and not from the vibrational ground state). A detailed description of this method is given in the Supporting Information.

This communication presents the first stimulated Raman investigations on isolated triphenylmethane-based dimers in the gas phase using our newly modified laser setup (see section 1.2, Supporting Information). The capability of the applied techniques is demonstrated by clearly identifying the isolated dimer structures exhibiting structurally sensitive, Raman-active vibrations.

Figure 2 shows the ILSR spectrum of the $(TPM)_2$ mass trace in the aromatic C–H stretching region obtained via the electronic resonance of 37212 cm^{-1}, the R2PI spectrum of $(TPM)_2$ is depicted in Figure S24. In case of the TPM

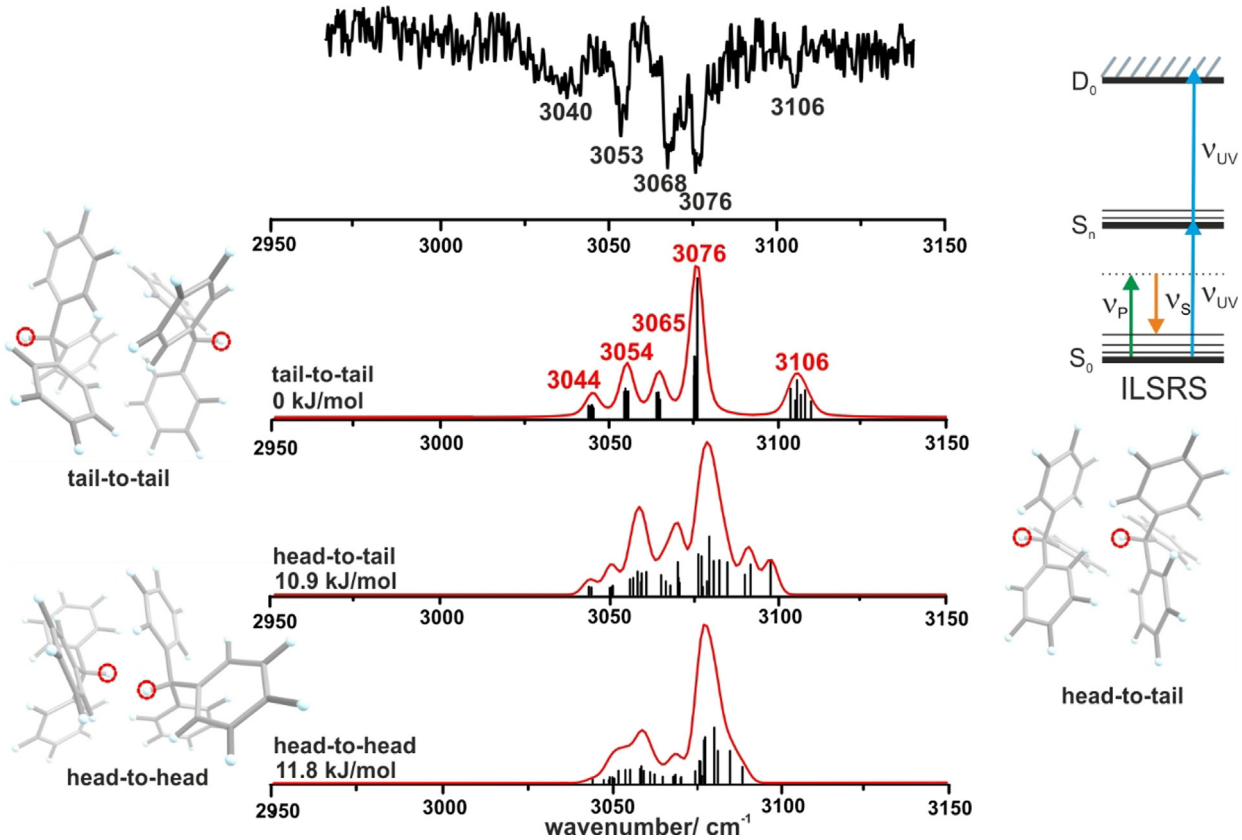

Figure 2. ILSR spectrum of $(TPM)_2$ in the aromatic C–H stretching region compared to calculated vibrational frequencies with Raman intensities at B3LYP-D3(BJ)/def2-TZVP level for the tail-to-tail, head-to-tail, and head-to-head arrangements, scaling factor 0.963 (arom. C–H); factor obtained with respect to CH vibrations of the TPM monomer (see Figure S25). The energy values refer to E_0, the relative BSSE-corrected energy of the respective dimer, including ZPVE. The calculated vibration spectra of the three different isomers all have the same intensity scale. The red dotted marks characterize the aliphatic C–H groups.

monomer it was possible to record the corresponding IGSR spectrum in the C–H stretching region (*cf.* Figure S25). These experimentally observed vibrational transitions in combination with DFT calculations are the basis for the structural assignments. There are tail-to-tail, head-to-tail, and head-to-head dimers (Figure 1). Despite the significantly lower S/N ratio, similarities of the ILSR spectrum (Figure 2) of the dimer to the IGSR spectrum of the TPM monomer (Figure S25) are obvious: With a difference of not more than 3 cm^{-1}, the transitions at 3041 (3040), 3052 (3053), 3068 (3068), and 3079 (3076) cm^{-1} occur in the monomer (and dimer) spectra, implying some symmetry for the TPM dimer as well. Merely the blue-shifted transition at 3106 cm^{-1} appears as a noticeable additional feature within the aromatic C–H stretching region of the dimer spectrum. Good agreement exists between the ILSR spectrum and the calculated vibrational frequencies including Raman intensities for the tail-to-tail arrangement in $(TPM)_2$ (Figure 2). Six aromatic C–H stretching vibrations are significantly blue-shifted compared to the remaining ones (*cf.* Section 2.1 in the SI). This is not observed for the head-to-tail and head-to-head arrangements. This significant difference in the tail-to-tail structure is due to a bond compression induced by the balance of Pauli repulsion and LD in the dimer (Figure 2). Furthermore, nearly degenerate frequencies in the symmetric tail-to-tail structure result in formation of four groups of C–H stretching frequencies leading to a structured ILSR spectrum with four peaks between 3000 and 3100 cm^{-1}. In case of the head-to-tail and head-to-head structures the remaining C–H stretching vibrations are much more spread. This spreading (resulting in a broadening of the spectrum) is not directly observed in the experimental spectrum. There are more possible arrangements which are in between the three limiting types but only for the symmetric tail-to-tail geometry a structured spectrum with a clearly separated group of C–H stretching vibrations at about 3106 cm^{-1} is obtained. The assignment of the tail-to-tail structure is further supported by IR/R2PI spectra in the aliphatic C–H region (*cf.* Figure S27). Despite this unambiguous assignment the presence of a small fraction (< 30 %) of the energetically strongly disfavored head-to-tail and head-to-head isomers due to kinetic trapping cannot be excluded since in this case their vibrational pattern would be hidden below the spectrum of the dominant tail-to-tail isomer.

Turning to $(T^tBuPM)_2$, head-to-head, head-to-tail, and tail-to-tail structures are shown in Figure 3 (see also Figures S7–S9 and S13–S15). The linear head-to-head structure observed in the crystal[19] exhibits an intermolecular C–H···H–C distance of 1.566(5) Å obtained by neutron diffraction at 20 K, the shortest intermolecular C–H···H–C distance measured to date. As there are no crystal packing effects influencing the structure in the gas phase, the structure is expected to be somewhat "relaxed" compared to the solid state, resulting in a slightly larger C–H···H–C distance of 1.571 Å (B3LYP-D3(BJ)/def2-TZVP). Compared to the head-to-head arrangement the competing head-to-tail and

Table 1: Relative energies for $(T^tBuPM)_2$ obtained at different computational levels. The ΔE-values and D_0-values refer to BSSE-corrected values for the deuterated dimer. All values are given in kJ mol^{-1}.

	B3LYP-D3(BJ)/def2-TZVP			B97-D/def2-TZVP		
	ΔE	ΔE_0	D_0	ΔE	ΔE_0	D_0
head-to-head	0	0	115.3	0	0	110.5
head-to-tail	22.8	28.5	86.8	11.8	14.0	96.5
tail-to-tail	68.6	67.2	48.2	51.6	46.7	63.8

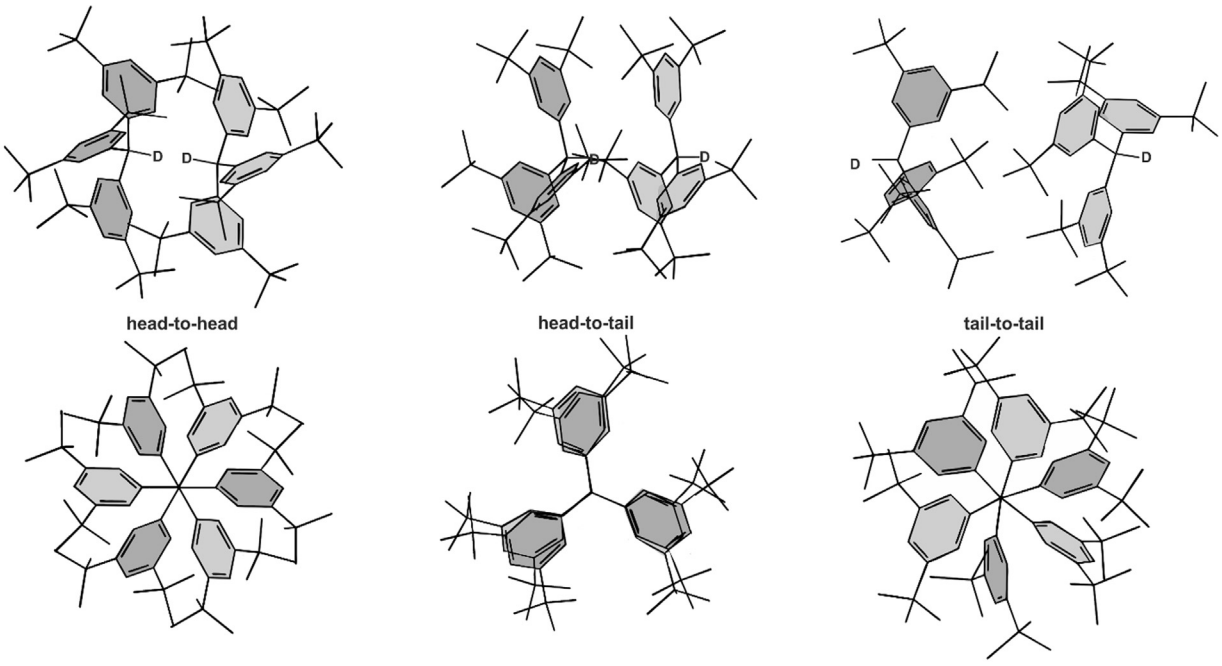

Figure 3. Computed three geometries for the all-*meta tert*-butyl triphenylmethane dimer $(T^tBuPM)_2$ at B3LYP-D3(BJ)/def2-TZVP. In the second row the view in direction of the C–D···D–C bond of the head-to-head, head-to-tail and tail-to-tail structure are depicted.

tail-to-tail structures are energetically disfavored (Table 1). This results from the sterically demanding *tert*-butyl moieties in $(T^tBuPM)_2$ leading to a larger distance between the phenyl rings and thus a lack of interaction surface compared to the head-to-head arrangement. Within the head-to-head structure, the *tert*-butyl moieties enable an ideal interlocking between the two T^tBuPM molecules in which LD is able to outbalance Pauli repulsion.

To obtain a structural identification of $(T^tBuPM)_2$ a vibrational analysis of the C–H stretching modes has been performed. The two C–H stretching vibrations of the dimer involving the C–H moieties at the central carbon atom of each TPM unit should be structurally sensitive with respect to the head-to-head, head-to-tail, and tail-to-tail arrangements. The remarkably short C–H···H–C distance in the head-to-head arrangement should create a unique structural identifier differing from all other arrangements. Remarkably large Raman intensities are theoretically predicted especially for the plethora of aliphatic C–H stretching vibrations (*cf.* Figure S10). Unfortunately, the structurally sensitive C–H vibrations overlap with parts of the aliphatic C–H stretching modes of the 12 *tert*-butyl groups (*cf.* Figure S10). This problem is solved by preparing and investigating the singly deuterated T^tBuPM and its dimer, in which a deuterium atom replaces the hydrogen atom of the central C–H moiety. The C–D vibrations shift to a spectral region around 2200 cm^{-1} where no spectral overlaps are expected.

The two aliphatic C–D stretching vibrations of the tail-to-tail and head-to-tail isomers calculated harmonically at B3LYP-D3(BJ)/def2-TZVP are completely localized. The head-to-head arrangement (almost S_6-symmetry) displays a Raman-active (IR-inactive) symmetric and a Raman-inactive (and vanishingly small IR active) asymmetric stretching normal mode of the two coupled C–D vibrations. Thus, the stimulated Raman techniques are an ideal tool to investigate the asymmetric structure sensitive C–D vibration. For a better theoretical description of the symmetric C–D stretching mode, a one-dimensional potential energy curve along the normal coordinate (*cf.* Figures S18–S23) was computed at B3LYP-D3(BJ)/def2-TZVP. The same procedure has been performed for the localized C–D vibrations of the tail-to-tail and head-to-tail isomers (Figures S21 and S23). The calculations confirm the assumption that the symmetric C–D vibration in the head-to-head dimer is significantly blue-shifted compared to the isolated C–D vibrations in the other dimers (Figure 4).

The demanding ILSR method could be applied with respect to the isolated C–D vibrations. The experimentally obtained spectrum (recorded via an UV excitation at 36958 cm^{-1}, Figure S28) is given in Figure 4 and is compared to the computed data. A strong transition at 2270 cm^{-1} and a weaker one at 2134 cm^{-1} are observed in the ILSR spectrum. The band at 2270 cm^{-1} is strongly blue-shifted in agreement with the prediction for the head-to-head structure and in contrast to the C–D frequencies computed for the other dimer structures (Figure 4; Tables S6 and S8; Figures S12 and S17). Thus, in agreement with the theoretical prediction, the strong transition at 2270 cm^{-1} can unambiguously be assigned to the most stable head-to-head structure, clearly indicating its formation under isolated conditions.

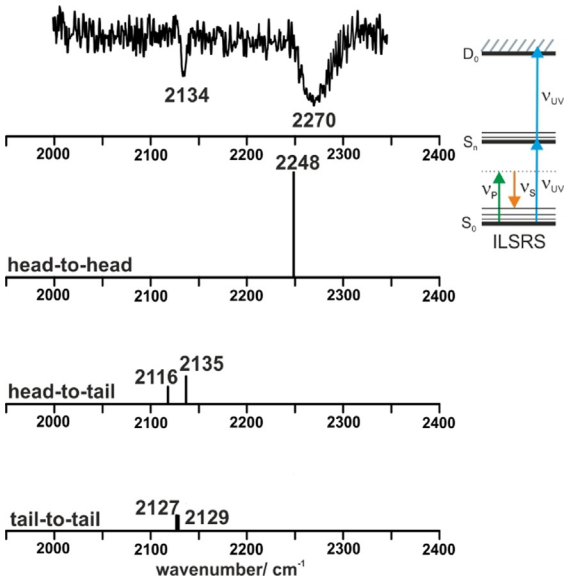

Figure 4. ILSR spectrum of $(T^tBuPM\text{-}d_1)_2$ in the region of the aliphatic C–D stretching vibrations compared to the calculated anharmonic values (obtained from one-dimensional potential energy curves along the normal coordinates at B3LYP-D3(BJ)/def2-TZVP, see text and Figures S18–S23). The computed relative Raman intensities (arbitrary units) are taken from the normal mode analyses and are indicated by the heights of the bars. The calculated vibration spectra of the three different isomers all have the same intensity scale.

The second sharper transition at 2134 cm^{-1} could originate from a C–D bending overtone of the central aliphatic carbon atoms of the T^tBuPM moieties (see section 3.2 in the SI). Coupled bending vibrations are calculated at 1062 and 1065 cm^{-1} (harmonic approximation, B3LYP-D3(BJ)/def2-TZVP, scaled by 0.99[20]). However, another explanation for the transition at 2134 cm^{-1} is that it arises from the tail-to-tail isomer (as an overlap of the two C–D frequencies which are almost identical). It would also be possible that the vibrations of the tail-to-tail structure and one of the more stable head-to-tail arrangement overlap (the remaining transition of the head-to-tail structure may be too weak to be observed). The formation of the energetically disfavored head-to-tail and/or tail-to-tail isomers, which can hardly be distinguished from the head-to-head isomer by their UV resonance might be explained by kinetic trapping during the supersonic expansion (*cf.* Section 3.2 of the SI).

The main goal of this communication is to demonstrate that the linear head-to-head arrangement in $(T^tBuPM)_2$ observed in the condensed phase is also found under isolated conditions in the gas phase. Ionization loss stimulated Raman experiments unambiguously identify the structure through the Raman-active C–D vibration of the dimer composed of monodeuterated monomers. This vibration is characteristically blue-shifted compared to competing structures due to significant C–H(D) bond compression in this peculiar dimer arrangement involving an extremely short C–H(D)···(D)H–C distance. In $(TPM)_2$ Pauli repulsion exceeds LD attraction when the two TPM moieties approach each other head-to-

head, leading to the preference of the tail-to-tail structure. By introducing the *tert*-butyl substituents as large DEDs, the balance is tipped towards LD attraction within the head-to-head arrangement. The clear spectroscopic identification of the $(T^tBuPM)_2$ structure in the gas phase proves that crystal packing effects play a negligible role for the observed head-to-head arrangement in the condensed phase. Thus, this text book example shows that the arrangement is driven by LD originating from a multitude of *tert*-butyl groups outbalancing steric repulsion. In unsubstituted $(TPM)_2$ no comparable LD stabilization is possible and a tail-to-tail structure forms. Likewise, this study demonstrates the remarkable ability of stimulated Raman techniques within molecular beam experiments to elucidate the structure of large, symmetric, and nonpolar molecular aggregates by their Raman-active vibrations.

Acknowledgments

The authors would like to acknowledge funding from the Deutsche Forschungsgemeinschaft (DFG, Ge 961/9-2 and Schr 597/27-2) within the priority program SPP 1807 "Dispersion" for funding. Furthermore the authors thank Prof. C. van Wüllen for performing part of the dimer calculations on his high performance computer cluster. The authors also want to thank PD C. Riehn and Dr. K. Schwing for the fruitful discussion. This work is part of the doctoral thesis of D.M. and P.H.S. Open access funding enabled and organized by Projekt DEAL.

Conflict of interest

The authors declare no conflict of interest.

Keywords: combined IR/UV experiments · density functional theory · molecular beam experiments · non-covalent interactions · vibrational spectroscopy

[1] F. London, *Z. Phys.* **1930**, *63*, 245 – 279.
[2] J. P. Wagner, P. R. Schreiner, *Angew. Chem. Int. Ed.* **2015**, *54*, 12274 – 12296; *Angew. Chem.* **2015**, *127*, 12446 – 12471.
[3] A. J. Stone, *The theory of intermolecular forces*, Oxford Univ. Press, Oxford, **2013**.
[4] S. Hanlon, *Biochem. Biophys. Res. Commun.* **1966**, *23*, 861 – 867.
[5] *Advances in Protein Chemistry* (Eds.: S. K. Burley, G. A. Petsko), Academic Press, New York, **1988**.
[6] K. Autumn, M. Sitti, Y. A. Liang, A. M. Peattie, W. R. Hansen, S. Sponberg, T. W. Kenny, R. Fearing, J. N. Israelachvili, R. J. Full, *Proc. Natl. Acad. Sci. USA* **2002**, *99*, 12252 – 12256.
[7] L. Goerigk, S. Grimme, *Phys. Chem. Chem. Phys.* **2011**, *13*, 6670 – 6688.
[8] a) P. R. Schreiner, L. V. Chernish, P. A. Gunchenko, E. Y. Tikhonchuk, H. Hausmann, M. Serafin, S. Schlecht, J. E. P. Dahl, R. M. K. Carlson, A. A. Fokin, *Nature* **2011**, *477*, 308 – 311; b) A. A. Fokin, L. V. Chernish, P. A. Gunchenko, E. Y. Tikhonchuk, H. Hausmann, M. Serafin, J. E. P. Dahl, R. M. K. Carlson, P. R. Schreiner, *J. Am. Chem. Soc.* **2012**, *134*, 13641 – 13650.
[9] S. Rösel, J. Becker, W. D. Allen, P. R. Schreiner, *J. Am. Chem. Soc.* **2018**, *140*, 14421 – 14432.
[10] a) S. Rösel, C. Balestrieri, P. R. Schreiner, *Chem. Sci.* **2017**, *8*, 405 – 410; b) N. Yannoni, B. Kahr, K. Mislow, *J. Am. Chem. Soc.* **1988**, *110*, 6670 – 6672.
[11] S. Grimme, P. R. Schreiner, *Angew. Chem. Int. Ed.* **2011**, *50*, 12639 – 12642; *Angew. Chem.* **2011**, *123*, 12849 – 12853.
[12] B. Kahr, D. van Engen, K. Mislow, *J. Am. Chem. Soc.* **1986**, *108*, 8305 – 8307.
[13] M. Gomberg, *J. Am. Chem. Soc.* **1900**, *22*, 757 – 771.
[14] H. Lankamp, W. T. Nauta, C. MacLean, *Tetrahedron Lett.* **1968**, *9*, 249 – 254.
[15] a) E. G. Robertson, M. R. Hockridge, P. D. Jelfs, J. P. Simons, *J. Phys. Chem. A* **2000**, *104*, 11714 – 11724; b) E. G. Robertson, J. P. Simons, M. Mons, *J. Phys. Chem. A* **2001**, *105*, 9990 – 9992; c) P. Çarçabal, R. T. Kroemer, L. C. Snoek, J. P. Simons, J. M. Bakker, I. Compagnon, G. Meijer, G. v. Helden, *Phys. Chem. Chem. Phys.* **2004**, *6*, 4546 – 4552; d) T. S. Zwier, *Annu. Rev. Phys. Chem.* **1996**, *47*, 205 – 241; e) S. Tanabe, T. Ebata, M. Fujii, N. Mikami, *Chem. Phys. Lett.* **1993**, *215*, 347 – 352; f) C. Riehn, C. Lahmann, B. Wassermann, B. Brutschy, *Chem. Phys. Lett.* **1992**, *197*, 443 – 450; g) R. H. Page, Y. R. Shen, Y. T. Lee, *J. Chem. Phys.* **1988**, *88*, 4621 – 4636; h) M. Gerhards, C. Unterberg, *Phys. Chem. Chem. Phys.* **2002**, *4*, 1760 – 1765.
[16] G. Eckhardt, R. W. Hellwarth, F. J. McClung, S. E. Schwarz, D. Weiner, E. J. Woodbury, *Phys. Rev. Lett.* **1962**, *9*, 455 – 457.
[17] a) M. Felker, P. M. Maxton, M. W. Schaeffer, *Chem. Rev.* **1994**, *94*, 1787 – 1805; b) G. V. Hartland, B. F. Henson, V. A. Venturo, R. A. Hertz, P. M. Felker, *J. Opt. Soc. Am. B* **1990**, *7*, 1950.
[18] a) P. Esherick, A. Owyoung, J. Plíva, *J. Chem. Phys.* **1985**, *83*, 3311 – 3317; b) P. Esherick, A. Owyoung, *Chem. Phys. Lett.* **1983**, *103*, 235 – 240.
[19] S. Rösel, H. Quanz, C. Logemann, J. Becker, E. Mossou, L. Cañadillas-Delgado, E. Caldeweyher, S. Grimme, P. R. Schreiner, *J. Am. Chem. Soc.* **2017**, *139*, 7428 – 7431.
[20] a) C. W. Bauschlicher, S. R. Langhoff, *Spectrochim. Acta Part A* **1997**, *53*, 1225 – 1240; b) M. D. Halls, J. Velkovski, H. B. Schlegel, *Theor. Chem. Acc.* **2001**, *105*, 413 – 421; c) P. Sinha, S. E. Boesch, C. Gu, R. A. Wheeler, A. K. Wilson, *J. Phys. Chem. A* **2004**, *108*, 9213 – 9217; d) K. Bartl, A. Funk, K. Schwing, H. Fricke, G. Kock, H.-D. Martin, M. Gerhards, *Phys. Chem. Chem. Phys.* **2009**, *11*, 1173 – 1179.

Manuscript received: December 1, 2020
Revised manuscript received: February 13, 2021
Accepted manuscript online: March 11, 2021

